Functional-segregated coumarin-containing telodendrimer nanocarriers for efficient delivery of SN-38 for colon cancer treatment

Gaofei Xu[a,b,1], **Changying Shi**[a,1], **Dandan Guo**[a], **Lili Wang**[a], **Yun Ling**[b], **Xiaobing Han**[a], and **Juntao Luo**[a,*]

[a]Department of Pharmacology, SUNY Upstate Medical University, Syracuse, NY, 13210 United States

[b]Department of Applied Chemistry, Science College, China Agricultural University, Beijing, 100193, China

Abstract

Four coumarin-containing telodendrimers (denoted as P-I, P-II, P-III and P-IV) were designed and synthesized to self-assemble into the corresponding nanoparticles. Of those, two nanoparticles (P-II and P-IV micelles) were screened and selected for targeted drug delivery of 7-ethyl-10-hydroxy camptothecin (SN-38), a prominent and efficacious anticancer agent, for the treatment of colon cancers. The nanoparticle encapsulation significantly increased the solubility of SN-38 in aqueous solution. Dynamic light scattering (DLS) showed the size of these SN-38 nanoparticles to be around 50 nm, and rod-shaped micelles were observed using transmission electron microscopy (TEM). These two novel nanoformulations of SN-38/P-II and SN-38/P-IV were found to exhibit similar *in vitro* cytotoxic activity against colon cancer cells as the free drug (SN-38 in DMSO) and were 500-fold more potent than Irinotecan (a prodrug of SN-38). In addition, near infrared fluorescent (NIRF) optical imaging was utilized to monitor the tumor targeted delivery of SN-38/NPs via co-loading a NIRF dye. It was demonstrated that these NPs preferentially accumulated in tumors when compared to healthy tissue. A pharmacokinetics study showed that SN-38 micelle formulations had a longer circulating time in blood than Irinotecan. Furthermore, SN-38 loaded nanoformulations exhibit superior anti-tumor efficacy when compared with Irinotecan at equivalent SN-38 dose in HT-29 human colon cancer xenograft models.

Graphical abstract

*To whom correspondence should be addressed: luoj@upstate.edu; Fax: 1-315-464-5143; Phone: 1-315-464-7965.
[1]These authors have the same contributions in this study
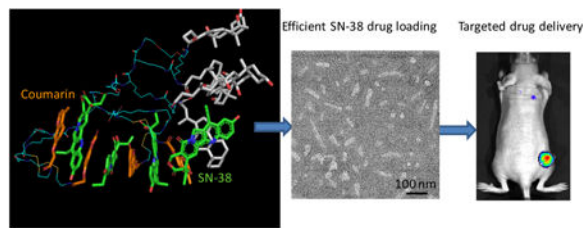
Keywords

Micelles; Irinotecan; SN-38; Drug delivery; Nanomedicine; Colon cancer

1. Introduction

Cancer remains a cause of considerable morbidity and mortality worldwide, recently surpassing heart disease as the leading cause of death in the US population younger than 85 years old. Colon cancer is a neoplastic disease of the large intestine, one of the most common malignancies in the western world with more than one million new cases each year and a disease-specific mortality rate of about 33%.[1] Although death rates are decreasing in the most developed countries owing to screening programs and therapy, colon cancer still holds third place in cancer death statistics for women and second for men.[2] Chemotherapy is an important treatment option for cancer patients. However the specific delivery of chemotherapeutic drugs to tumors is still a major hurdle in eradicating cancers. The continual development of drug delivery technologies is vital to future breakthroughs in chemotherapy.

Irinotecan (CPT-11), a topoisomerase I inhibitor, has been approved as the first-line chemotherapy drug for colorectal cancer in combination with a 5-fluorouracil/leucovorin/oxaliplatin (FOLFOX) regimen or as a monotherapy for second-line therapy following a failed FOLFOX regimen.[3] 7-Ethyl-10-hydroxy-camptothecin (SN-38) is a biologically active form of irinotecan upon the hydrolysis by carboxylesterases in the liver and in tumors. SN-38 is approximately 100-1000-fold more potent against various cancer cells than CPT-11.[4-8] Although irinotecan has demonstrated efficacy in practice, it is highly inefficient in delivering active SN-38 to tumor tissue. Studies in humans have shown that only 2-8% of the administered dose of irinotecan is actually converted to SN-38.[9] In addition, up to 95% of SN-38 is bound to circulating proteins such as albumin, which drastically reduces its bioavailability.[10] Another problem linked to CPT-11 in clinical use is its severe gastrointestinal toxicity and myelosuppression, which constitute its dose limiting toxicity (DLT).[11] The limitations of irinotecan make SN-38, with its high potency, an attractive molecule for anticancer drug development in colon cancer treatment. However, SN-38 is virtually insoluble in all pharmaceutically acceptable solvents and is unable to be used directly to treat patients.[12] The development of enhanced SN38 delivery systems would allow more efficient and safe treatment.

Nanoparticles with long circulation times have potential to accumulate in tumor tissue through the often leaky vasculature by the well known enhanced permeability and retention (EPR) effect. More than 40 nanomedicines have been approved for clinical use in the past

two decades and among those ∼25% were for the delivery of chemotherapeutics.[13] Additionally, more than 40 nanomedicine formulations for chemotherapy are currently in various stages of clinical development.[13] In recent years, a number of nanoparticle drug delivery systems, *e.g.* amphiphilic macromolecular prodrugs,[14-15] liposome formulation, [16] dendrimers[17] and polymer micelle formulations[18-19] of SN38 have been investigated for improved delivery to cancer cells and tissues. Although promising progress has been made in SN38 delivery in the literature, the clinical evaluation of these SN38 nanoformulations has been limited, creating a need for further investigation. The ultra-flat aromatic structure of SN38 tends to "sneak out" from nanocarriers to form precipitation or induce large aggregation, which hinders the *in vivo* application. NK012 is a polymeric prodrug of SN38 based on PEG-poly(glutamic acid) and currently is under clinical trials, [20-21] which could assemble into micelles for the targeted drug delivery. However, it still relies on enzymatic or chemical cleavage similar to irinotecan, which may reduce the efficacy in treating cancers.

Compared with dendrimers, liposomes and other organic/inorganic nanoparticles, polymeric micelles are much more versatile to deliver a broad spectrum of therapeutics due to their enormous chemical variation, relative easy preparation, multiple functionality and high drug loading capacity.[22-25] Due to their unique size range (10–100 nm), micelles are able to avoid renal clearance with the minimized liver and spleen uptake. These micelles also preferentially accumulate in solid tumors via the EPR effect.[26] In our previous studies, we have designed and synthesized a unique class of well-defined amphiphilic linear-dendritic block copolymers (named as telodendrimer) by stepwise peptide condensation approach. Telodendrimers are composed of linear poly(ethylene glycol) (PEG), dendritic polylysine and specific peripheral groups, which self-assemble into nanocarriers for efficient drug delivery.[27-32] Herein, we rationally designed and developed a series of novel nanocarriers by introducing bio-sourced aromatic coumarin on the periphery of telodendrimer. The inclusion of coumarin is expected to interact with SN-38 via pi-pi stacking and therefore optimize the drug loading capacity and stability.

2. Materials and methods

2.1 Materials and instruments

SN-38 was purchased from AK Scientific, Inc. (Union City, CA, USA). Mono-methyl terminated poly(ethylene glycol) monoamine (MeO-PEG-NH$_2$, M.W.: 5000 Da) was purchased from JenKem Technology, USA Inc. (Allen, TX, USA). (Fmoc)Lys(Boc)-OH and (Fmoc)Lys(Fmoc)-OH were purchased from AnaSpec Inc. (San Jose, CA. USA). 1-Hydroxybenzotriazole (HOBt, 98%) and N,N′-Diisopropylcarbodiimide (DIC, 99%) were obtained from Acros Organics. The MALDI matrix α-Cyano-4-hydroxycinnamic acid was purchased from Sigma Aldrich Chemical Co. 1,1′-dioctadecyl-3,3,3′,3′-tetramethylindodicarbocyanine perchlorate (DiD), a hydrophobic near infrared fluorescence dye and 1,1-Dioctadecyl-3,3,3,3- tetramethylindocarbocyanine perchlorate (DiI) were purchased from AAT Bioquest, Inc. (Sunnyvale, CA). CellTiter 96® AQ$_{ueous}$ MTS reagent powder was purchased from Promega (Madison, WI, USA). Cholic acid and all other chemical reagents were purchased from Sigma-Aldrich. Dialysis membrane with MWCO of

3500 Da was purchased from Spectrum Laboratories, Inc. A disulfide bond containing linker molecules was synthesized following the procedure reported in a literature.[33] Proton NMR spectra were recorded on a Bruker AVANCE 600 MHz spectrometer. Mass spectra were acquired using a Bruker REFLEX-III MALDI-TOF mass spectrometer, equipped with a nitrogen laser delivering 3 ns laser pulses at 337 nm. SN-38 concentration was measured by a Hitachi F-4500 Fluorescence Spectrophotometer.

The nomenclature of the telodendrimers followed the system used in the previous studies: For example, telodendrimer $PEG^{5K}Co_8$ indicates that the molecular weight of PEG is 5 kDa and there are 8 coumarin conjugated on the periphery of dendritic polylysine, three layer telodendrimer PEG^{5K}-CA_4-LO-LS_4Co_4 indicates that four coumarin conjugated on the periphery via linker molecules containing S-S bonds (LS), and four cholic acid conjugated in the middle layer of the dendritic polylysine and a triethylene glycol linker (LO) molecule was inserted between two layers. Among the abbreviations are PEG (poly(ethylene glycol)), CA (cholic acid), Co(coumarin), the disulfide linker (LS) and triethyleneglycol linker (LO).

2.2 Synthesis of coumarin carboxylic acid derivative

The coumarin-based carboxylic acid was synthesized according to literature[34] with some modification. The detailed synthesis procedure was as follows: 2-Bromoactic acid (7.9 g, 56.8 mmol), 7-hydroxy-4-methylcoumarin (2.0, 11.4 mmol), potassium carbonate (15.7 g, 113.8 mmol), a trace of potassium iodide and 200 mL of ethanol were placed into a 500 mL round bottom flask equipped with a magnetic stir and refluxed for 20 h. The mixture was then poured into 200 mL of water, followed by pH adjustment to a value of ∼ 5 by addition of hydrochloric acid (5 wt %). The ethanol in the mixture was next evaporated at room temperature until a precipitate appeared. The final product was obtained at 85% yield by filtration and washed three times with water. ^{1}H NMR (600 MHz, DMSO-d_6): δ 7.7 (d, J = 7.7 Hz, 1 H, Ph-H), 6.97 (dd, J = 8.7, 2.7 Hz, 1 H, Ph-H), 6.93 (d, J = 2.5 Hz, 1 H, Ph-H), 6.22 (s, 1 H, C=CH), 4.79 (s, 3 H, CH3).

2.3 Synthesis of Telodendrimers

The telodendrimers containing the coumarin derivative (namely as P-I: $PEG^{5K}Co_8$, P-II: PEG^{5K}-CA_4-LO-Co_4, P-III: PEG^{5K}-CA_4-LO-LO_4Co_4 and P-IV: PEG^{5K}-CA_4-LO-LS_4Co_4 respectively; nomenclature: name the abbreviations: PEG (poly(ethylene glycol), CA(cholic acid), LO, LS, Co(coumarin)) were synthesized using a solution-phase condensation reaction starting from MeO-PEG-NH_2 (5000 Da) via stepwise Fmoc peptide chemistry following the previous procedure.[29, 31] The typical synthesis of PEG^{5K}-CA_4-LO-Co_4 was as follows:

(Fmoc)Lys(Boc)-OH was coupled onto the terminal amino group on PEG using DIC (3 equivalent) and HOBt (3 equivalent) as coupling reagents at room temperature until a negative Kaiser test result (yellow) was obtained indicating the completion of the coupling reaction. PEGylated molecules were precipitated by pouring reaction solution into excess amounts of cold ether, followed by centrifugation and then three times of washes with cold ether. The white powder precipitate was dried under reduced pressure and the Fmoc protecting group was removed using 20% 4-methyl piperidine solution in DMF. Second

coupling of (Fmoc)Lys(Boc)-OH was performed to react with the free amino group on polymer. After the removal of Fmoc groups, Fmoc protected triethylene glycol linker molecule was coupled to the terminal amino groups. Then two respective coupling of (Fmoc)Lys(Fmoc)-OH were carried out to subsequently generate a dendritic polylysine terminated with four Fmoc groups and two Boc-protected amino groups at the adjacent sites of polymer. PEG^{5K}-(NH-Boc)$_4$-(NH-Fmoc)$_4$ was obtained via coupling of (Boc)lys(Boc) onto the adjacent amino groups of the telodendrimers after removal of two Boc groups with 50% (v/v) trifluoroacetic acid (TFA) in dichloromethane (DCM). After the deprotection of Fmoc groups, coumarin-based acid, was then coupled to the terminal end of dendritic polylysine. Finally cholic acid NHS ester was coupled to the adjacent amino groups of dendritic polylysine after removal of Boc group.

The obtained product was purified via dialysis against pure water for three days. Dialysis media was refreshed every 4 h. ^{1}H NMR spectra of the polymers were recorded on a Bruker 600 MHz Nuclear Magnetic Resonance Spectrometer using DMSO-d_6 as the solvent. MALDI-TOF MS spectra of telodendrimers were recorded on a Bruker REFLEX-III instrument. The hydrodynamic diameters (Dh) of the micelles were determined by dynamic light scattering (DLS) on a Zetatrac Nano System. The emulsions were passed through 0.22 μm filters before DLS measurements. Each set of Dh values constituted in the average of triplicate measurement.

2.4 Characterizations of micelles

To visualize the micelles by transmission electron microscopy (TEM), micelle solutions in dd-water were dropped onto 200 mesh copper grids, coated with carbon film, for 1 min and then the droplet was removed by filter paper. Subsequently, a drop of uranyl acetate solution was dropped immediately onto the copper grids for 1 min to stain the sample grids. Then staining solution was removed completely via filter paper and air dried before observed under a JEOL JEM-2100 HR instrument operating at a voltage of 200 kV. The size and size distribution of the micelles were measured by dynamic light scattering (DLS) instruments (Nanotrac). The micelle concentrations were kept at 5 mg/mL for DLS measurements. To evaluate the storage stability of the prepared NPs, the micellar solutions were incubated at room temperature and the particle sizes was monitored by DLS over time.

2.5 Critical micelle concentration (CMC)

The typical CMC measurement of P-II was conducted as follows: P-II was dissolved in PBS buffer under sonication. The initial micelle solution was diluted with PBS to obtain the required series solutions ranging from 0.4 to 200 μg/mL. To determine the CMC of P-II, a known amount of Nile Red in MeOH was added to a series of vials. When MeOH was evaporated under vacuum, a measured amount of P-II solution was added to each vial to obtain a final concentration of 1μM Nile Red and shake overnight in dark at room temperature. The fluorescence emission intensity was measured at the wavelength of 620 nm (excited at 543 nm) using a microplate reader (Synergy™ 2, BioTek Instruments, Inc.). CMC was determined at the intersection of the tangents to the two linear portions of the curve of the fluorescence intensity as a function of P-II concentration.

2.6 Preparation of SN-38 loaded micelles

An evaporation method was used for SN-38 loading. SN-38 was dissolved in mixed solution of chloroform and methanol (v/v, 9/1), then PEGylated polymer were dissolved with the SN-38 solution. The organic solvent was evaporated under vacuum to form a thin film. PBS buffer was added to hydrate the film, followed by 2 h of sonication and then the micelles solution was passed through a 0.22 μm filter. The final concentrations of the polymers were maintained at 5 mg/mL for all the drug-loading tests. The amount of drug loaded in the micelles was analyzed by measuring fluorescence intensity after 200 times dilution of the drugs loaded micelles with DMF. The fluorescence quantification was conducted on fluorescence spectrophotometer F-4500 (Hitachi, Japan). The emission intensity at 427 nm was recorded with an excitation wavelength at 372 nm. The drug loading capacity (DLC) and drug loading efficiency (DLE) were defined by the following equations: $DLC(\%) =$ [weight of SN-38/(weight of SN-38+weight of polymer)] $\times 100\%$, DLE (%) =(weight of SN-38 in the micelles/total weight of SN-38 in the loading solution) $\times 100\%$.

2.7 In vitro stability and drug release

The stability of produced SN-38-loaded micelles was evaluated upon storage at 4 Cover months and the particle size and distribution was measured via DLS over time. Release of SN-38 from a dialysis tube (MWCO: 3500 Da) was measured via fluorescence spectrometer. A 4 L PBS (1 ×) at pH 7.4 was used as a medium at room temperature under gentle stirring. SN-38 loaded polymeric micelles with 5:0.5 weight ratio of the polymer to SN-38 were prepared in PBS solution, 500 μL of these drug solutions were placed in a dialysis bag (MWCO: 3500 Da) and immersed in the medium. The concentration of SN-38 remaining in the triplicate dialysis bag at various time points was measured by fluorescence spectrophotometer.

2.8 Molecular Dynamic Simulation

The chemical structures of the telodendrimers P-II and P-IV and the drug molecule SN-38 were built using Maestro 9.7 (Schrodinger software). To reduce the computational time, the telodendrimer structure was designed to contain three ethylene glycol units only. Each SN-38/telodendrimer system contained four SN38 drug molecule and one telodendrimer molecule to mimic the drug loading content in the experiment. In the complex system telodendrimer and drugs molecules were randomly located in the simulation box using Maestro. All MD simulations were carried out using Desmond software package (Desmond/Maestro academic version 2014.2)[35-36] and analyzed with Maestro's trajectory visualizer. For each MD simulation, the default OPLS-2005 force field was used for all molecules of the system, the water box type was orthorhombic and the water molecules were modeled with simple point charge (SPC) model [37]. In the minimization process all molecules of telodendrimer, drug and water are allowed to minimize and relax their position. Ion neutralization process was applied to check and balance the charge of the system. In the main MD simulations, the smooth PME (Particle-mesh Ewald)[38] was used to treat long-range coulombic interactions, the system was equilibrated in an NPT ensemble with Nose-Hoover thermostat method at 300K.The time step was set at 2 fs and a 9 Å cut-off was used

for non-bonded interactions. The MD production run was carried out for 10 ns using Langevin dynamic to keep the temperature and pressure at the default value of Desmond.

2.9 Photo crosslinking and de-crosslinking of micelles

P-II and P-IV telodendrimer micelles in PBS at 1 mg/mL were irradiated using UV light (Dymax Bluewave 200, UVA, 100 mW/cm^2), or UV lamp (= 254 nm, 4 watts) for micelle crosslinking and de-crosslinking, respectively. The crosslinking degree of micelles was characterized using UV-Vis spectrometer via monitoring the percentage of the decay of the characteristic absorbance of coumarin at 320 nm compared with the initial intensity.[39]

2.10 Hemolysis

1 mL of fresh blood from healthy human volunteer was collected into 10 mL of PBS solution in the presence of 20 mM EDTA. Red blood cells (RBCs) were then separated by centrifugation at 1000 g for 10 min. The RBCs were washed three times with 10 mL of PBS, and re-suspended in 20 mL PBS. 200 μL of diluted RBC suspension was incubated with polymers at a series of concentrations (10, 100, 500 and 1000 μg/mL) with gentle shake at 37 °C. After 0.5 h, 4 h and overnight, the mixtures were centrifuged at 1000 g for 5 min. The free of hemoglobin in the supernatant was determined by measuring the absorbance at 540 nm using a UV-Vis spectrometer. Incubations of RBCs with Triton-100 (2%) and PBS were used as the positive and negative controls. The percent hemolysis of RBCs was calculated using the following formula: RBC Hemolysis = $100\% \times (OD_{sample} - OD_{PBS})/(OD_{triton} - OD_{PBS})$.

2.11 Cell culture

HT-29, HCT116 (colon cancer cell lines) and A549 (lung cancer cell line) were purchased from American Type Culture Collection (ATCC; Manassas, VA, USA). HT-29 and HCT116 cell lines were cultured in McCoy's 5A medium and A549 cell line was in DMEM medium supplemented with 10% fetal bovine serum (FBS), 100 U/mL penicillin G, and 100 μg/mL streptomycin at 37 °C using a humidified 5% CO_2 incubator.

2.12 Confocal fluorescence microscopy

DiI (a hydrophobic cyanine dye) was loaded together with SN-38 into the micelles to probe the nanoparticles in cell. HT-29 cells were seeded in chamber slide with a density of 5×10^4 cells per well and cultured for 24 h. Then cells were incubated with free DiI and DiI-SN38 loaded micelles at the final DiI concentration of 1 μg/mL at 37 °C. After 30 min or 2 h incubation, the cells were washed three times with cold PBS and fixed with 4% formaldehyde for 10 min. The cell nuclei were stained with 4′,6-diamidino-2-phenylindole (DAPI). The slides were mounted with coverslips and cells were imaged with a Nikon laser scanning confocal fluorescence microscopy.

2.13 Cell viability assay

Cells were seeded in 96-well plate a day prior to the treatment at a density of 3000 cells per well. After 72 h incubation with different concentrations of blank micelle and various formulations of SN-38 with different dilutions in a humidified 37 °C, 5% CO_2 incubator, a

mixture solution (CellTiter 96® Q_{ueous} MTS and an electron coupling reagent PMS) was added to each well and further incubated for 2 h at 37 °C. The cell viability was determined by measuring the absorbance of formazan at 490 nm using a microplate reader (BioTek Synergy 2). Untreated cells served as a control. Results were shown as the average cell viability [$(OD_{treat}−OD_{blank})/(OD_{control}−OD_{blank})×100\%$] of triplicate wells. The IC50 value was calculated as the concentration of agents that inhibited the cell growth by 50%.

2.14 Xenograft Mouse Model

Female athymic nude mice (Nu/Nu strain), 5-6 weeks age with an average body weight of 20 grams, were purchased from Harlan (Livermore, CA). All animals were kept under pathogen-free conditions according to AAALAC (Association for Assessment and Accreditation of Laboratory Animal Care) guidelines and were allowed to acclimatize for at least 4 days prior to any experiments. All animal experiments were performed in compliance with institutional guidelines and according to protocol approved by the Committee for the Humane Use of Animals of State University of New York Upstate Medical University. Subcutaneous colon cancer xenograft mouse model were established by injecting $1×10^7$ HT-29 cancer cells in a 100 μL of mixture of PBS and Matrigel (v/v, 1/1) without fetal bovine serum (FBS) subcutaneously at the right flank in female nude mice.

2.15 Fluorescence anima l imaging

Hydrophobic NIRF dye (DiD) was encapsulated together with SN-38 into the micelles using the same method as described above. The DiD-SN-38-coloaded micelles formulation was filtered with a 0.22 μm filter to sterilize the sample. Nude mice with subcutaneous tumors of approximate 8 to 10 mm in diameter were subjected to in vivo NIRF optical imaging. The HT-29 tumor xenografts bearing nude mice were injected with DiD-SN38-coloaded micelles with 10: 1: 0.2 ratio of polymer to SN-38 to DiD and free DiD via the tail vein, respectively. Then the mice anesthetized and optically imaged with an IVIS 200 (PerkinElmer) with the excitation at 625 nm and the emission at 700 nm, at different time points (0.5 h, 1 h, 2 h, 4 h, 8 h, 24 h, 48 h and 72 h). At the end of the experiment, the animals were sacrificed and all the major organs and tumor were excised for *ex vivo* imaging. The associated fluorescence intensities were determined by Living Image software (Caliper Life Sciences) using operator-defined regions of interest (ROI) measurements.

2.16 Pharmacokinetics study

Irinotecan and SN-38 loaded micelle were injected into female nude mice (8-10 weeks old) via tail vein at a single dose of 30 and 20 mg/kg body weight, respectively (n = 3 for each group). At different time points (5 min, 30 min, 1 h, 2 h, 4 h, 8 h, 24 h and 48 h) post injection, blood was collected in a heparinized tube. The blood was separated by centrifugation and plasma was isolated for the analysis. Twenty micro liters of plasma were added to 380 μL of DMF solvent, and SN-38 was extracted overnight at room temperature. The fluorescence of the supernatant was determined at excitation/emission of 372/424 nm to calculate SN-38 concentration.

2.17 In-vivo antitumor efficacy

Subcutaneous HT-29 xenograft mouse model was used to evaluate the therapeutic efficacy of different formulations of SN-38. Treatments were started when tumor in the nude mice reached a tumor volume of 150-300 mm^3 and this day was designated as day 0. On day 0, these mice were randomly divided into three groups (n = 5-6). Mice were intravenously administrated with PBS, Ironotecan HCl, and SN38-loaded micelles at the dose of 40 mg/kg SN-38 equivalent, respectively. The treatment was given every four day on days 0, 4 and 8 for total three doses. Tumor sizes were measured with a digital caliper 2-3 times per week. Tumor volume was calculated by the formula $(L \times W^2)/2$, where L is the longest, and W is the shortest in tumor diameters (mm). To compare between groups, relative tumor volume (RTV) was calculated at each measurement time point (where RTV equals the tumor volume at given time point divided by the tumor volume prior to initial treatment). For humane reasons, animals were sacrificed when the implanted tumor volume reached 1500 mm^3, which was considered as the end point of survival data. At day 7 after the last dosage, blood samples were obtained from all the mice for the measurement of blood cell counts.

2.18 Statistical analysis

Results were expressed as mean values ± SD. A Student's t-test was used for statistical comparison/analysis. The level of significance in all statistical analyses was set at a probability of $P < 0.05$.

3. Results and Discussion

SN38 has a five fused-ring structure with four aromatic rings forming a highly delocalized π-electron system with ultra-flat structure which easily form pi-pi stacking that precipitates out from water and even pharmaceutical solvents. To develop a stable formulation for SN-38, the recipient solvent or nanocarrier needs to bind to SN38 preferably to form stable dispersion of drug molecules. We have developed a series of telodendrimers with coumarin (Co) and cholic acid (CA) as peripheral groups, which self-assemble into micelles with UV sensitivity for reversible micelle crosslinking and de-crosslinking.[40] These coumarin-containing telodendrimers is expected to form pi-pi stacking with aromatic molecules, e.g. SN-38, and therefore encapsulate such kind drug efficiently within the micelles formed. However, the drug loading experiments revealed unsatisfactory loading properties of SN-38, such as low drug loading capacity and poor stability. A close examination of the telodendrimer structure found that the alternating CA and Co on the α- and ε- positions of polylysine (Supporting information Scheme S1) could possibly weaken the capability of pi-pi stacking of Co with SN-38. One could imagine that the sandwich structure would be the most stable pi-pi stacking system and it could effectively prevent the further aggregation of drug molecules from precipitation. A telodendrimer $PEG^{5K}Co_8$ (P-I, as shown in Scheme 1) with eight coumarin on the peripheral of telodendrimer was designed to maximize the coumarin-SN-38 interaction for better drug loading. At the same time, we have designed three-layered telodendrimers, P-II, P-III and P-IV with an adjacent branched oligo-CA between PEG and dendritic oligo-Co (Scheme 1). The insertion of the additional branched layer in polymer structure could benefit the phase segregation in the formation of micellar

structure. In addition, the proper linker molecule has been introduced in P-III and P-IV prior to Co conjugation providing necessary flexibility in binding with SN38.

3.1 Synthesis and Characterization

Telodendrimers have been synthesized via step-wise peptide chemistry (Supporting information Scheme S2). Polymers are designated as P-I ($PEG^{5K}Co_8$), P-II (PEG^{5K}-CA_4-LO-Co_4), P-III (PEG^{5K}-CA_4-LO-LO_4Co_4), and P-IV (PEG^{5K}-CA_4-LO-LS_4Co_4) respectively. P-I is comprised of linear PEG-blocking-dendritic oligo-coumarin, which has been synthesized following the reported procedure via Fmoc peptide chemistry.[29] The three-layered telodendrimers P-II, P-III, P-IV were synthesized via orthogonal protected Fmoc-Boc peptide chemistry. The scaffold intermediates of PEG^{5K}-$(NHBoc)_2$-LO-$(NHFmoc)_4$ PEG^{5K}-$(NHBoc)_4$-LO-$(NHFmoc)_4$ were characterized via ^1H NMR (supporting information Figure S1 & S2) to reveal their chemical structures, where the doubling of Boc signal was observed in the later compound after a $Lys(Boc)_2$-OH coupling I.

As shown in Figure 1, a clear detection of the aromatic protons of coumarin and methyl groups of cholic acid in telodendrimers in DMSO-d_6 allows the quantitative analysis of the chemical compositions. Interestingly, the protons on the oxylacetyl linkage of coumarin were split into two sets of peaks in P-I (Figure S3) and P-II (Figure 1), which were observed to be a single peak in P-III (Figure S4) and P-IV (Figure 1) with flexible spacers. This indicates the restricted molecular rotation of coumarin moieties in telodendrimers P-I and P-II, which may be due to the stereo-hindrance and the preferred pi-pi stacking of the adjacent coumarin molecules even in a good solvent of DMSO. The average numbers of CA and Co within these telodendrimers have been analyzed via the peak integrations of CA, e.g. three methyl groups on CA at 0.54, 0.77 and 0.88 ppm and the protons on the unsaturated carbons in Co at 6.19, 6.93 and 6.97 ppm, respectively, which were referenced to the signals on MeOPEG (CH_3: 3.27 and PEG: 3.47 ppm). As shown in Table 1, the chemical compositions of telodendrimers were calculated to be very close to the theoretical designs. Further, the molecular weights of telodendrimers were measured via MALDI-TOF MS, and the monomodal molecular weight distributions were observed for four telodendrimers (Figure 2A). As shown in Table 1, all the telodendrimers have very close molecular weight to the original design. The slightly less molecular weight detected in MS analysis were also consistent with the NMR detection.

The potential aggregation of telodendrimers may selectively suppress the signal of the core-forming segments in NMR analysis and cause the difficulty of flight for the high-molecular weight molecules in MALDI-TOF MS detection. Therefore, the solvent selection is very important in these measurements. As shown in Figure 2B, the proton signals of the hydrophobic domains in telodendrimers, including polylysine, were greatly suppressed in the NMR spectra in deuterated water. Only hydrophilic PEG could be detected with narrow peak width, which indicated the formation of the core-shell micelle structures. However, trace of signals of hydrophobic moieties in P-III could be detected in NMR spectrum (1-2.5 ppm and 6-8 ppm ranges in Figure 2B), indicating loose structure of micelles formed. This is due to the introduction of the hydrophilic triethylene glycol linkers in P-III, which is correlated with the highest CMC detected for P-III (4.5 μM, shown in Table 1) among

others. As a contrast, P-IV with extra hydrophobic disulfide bond linkers has a lowest CMC of 1.3 μM detected using Nile Red as a molecular probe.

All the telodendrimers in this study were observed to self-assemble into micelles with homogenous particle size distribution as detected by DLS (Figure 3). The P-III was observed to form smaller micelles with the size of 12 ± 2 nm. It is due to the presence of hydrophilic linkers in the structure, which reduce the hydrophobicity of the aggregates and increase the CMC compared to other telodendrimers (Figure S5). Other telodendrimers forms micelles with the particle sizes between 20 to 30 nm. After loaded with drug molecule SN-38 at a 1/10 mass ratio of drug/polymer, the particles sizes of P-II and P-IV were slightly increased to about 34 nm with the homogenous size distribution in DLS analysis. However, P-I and P-III showed significantly increased particle sizes and heterogeneity in size distribution after SN-38 loading (Figure 3). Transmission Electron Microscopy (TEM) imaging studies revealed the interesting morphology transformation between the empty and SN-38-loaded micelles. The P-II telodendrimer mainly forms into spherical particles with the particle size of ∼15-20 nm, which is slightly smaller than the DLS analysis due to the drying effects in TEM sample preparation. In addition, some fine nanofiberic objects were observed in P-II micelles in TEM preparation. P-IV telodendrimers mainly form rod shaped micelles before drug loading with the thickness of about 10 nm and length of ∼50-100 nm. The increased hydrophobic S-S spacers in P-IV than P-II causes the increased packing parameter (p) of telodendrimer, resulting in the switch of micelle morphology from spherical ($p < 1/3$) to rod shaped micelles ($1/3 < p < 1/2$).[41] After SN-38 loading, dominant rod shaped micelles were observed under TEM, which may be due to the increased pi-pi stacking between drug and polymer system. The similar thickness (10- 15 nm) and slightly reduced length of rod micelles were observed and some spherical micelles were also observed after SN38 loading under TEM.

3.2 Molecular dynamic simulation

P-II and P-IV form stable micelles with good drug loading properties, respectively. Therefore, both were studied in molecular dynamic simulation to understand the molecular packing in nanocarriers. In contrast, P-I and P-III both form large aggregates after drug loading (Figure 3). The atom level molecular dynamic simulation is not capable to simulate such aggregation event over hundreds of nanometers. Pi-pi stacking between SN38 and coumarin moieties within telodendrimer micelles is believed to be the key interaction in stabilizing drug molecules within nanocarrier. In order to illustrate the possible pi-pi stacking interactions between drug and core-forming building blocks, molecular dynamics (MD) were performed to simulate the complex of SN38 and the dendritic blocks of P-II and P-IV. Long PEG chain was eliminated in the MD study to accelerate the computational simulation. Four SN38 drug molecules and one dendritic unit were packed together into a simulation box, which was then filled with explicit water molecules. The 4:1 ratio of drug to telodendrimer was selected as it is close to the maximum capacity observed in drug loading assays. During a MD simulation over 10 ns, the core-forming building blocks aggregated together via solvophobic interactions, e.g. CA-CA hydrophobic interaction and Co-Co pi-pi stacking, to minimize hydrophobic exposure to water molecules (Figure 4). The hydrophobic interaction between CA-Co was also observed in empty P-II telodendrimer

(Figure 4e); whereas almost segregated CA and Co domains were observed in P-IV. Parallel and T-shaped pi-pi stacking of Co moieties were facilitated by the flexible linker molecules (Figure 4g), which may be expanded in the presence of multiple telodendrimers aggregation and induce the nanostructure in one-dimension growth. It was observed in TEM studies that P-IV has rod-shaped micelles (Figure 3). In contrast, the steric hindrance in P-II could interfere with formation of the long distance pi-pi stacking, therefore assembling into the 3-dimentional spherical micelles. After the addition of aromatic SN38, the pi-pi stacking was enforced as shown in MD simulation (Figure 4), which could explain the formation of the rod-shaped drug loaded micelles. Interestingly, Co-Co homo-stacking structures were observed to be preferred in P-II, which further interacts with SN-38 (Figure 4f). On another hand, long-distance alternating Co-SN38-Co pi-pi stacking were observed in SN38/P-IV system (Figure 4h), due to the flexible linker molecules.

3.3 Photo-crosslinking

We have demonstrated that the coumarin within telodendrimer could dimerize under UV-irradiation to crosslink micelles reversibly.[40] Therefore, the photosensitivity of these newly synthesized coumarin-containing telodendrimers need to be characterized. As shown in Figure 5A, the characteristic absorption of monomer coumarin at 320 nm decreased upon the exposure to UV light at > 310 nm, which indicate the dimerization of coumarin molecules.[42] Over 60% of dimerization could be achieved after 30 min UV exposure for P-II micelles. The dimerization could be dissociated reversibly upon the UV irradiation at 254 nm, which was evidenced by the recurrent of monomer coumarin absorbance at 320 nm (Figure 5B). Telodendrimer P-IV exhibited similar properties of the reversible photosensitive micelle crosslinking, except that a faster courmarin dimerization r rate (>70% dimerization over 13 min UV exposure, Figure S6) was observed under the same concentration (2 mg/mL) and UV exposure intensity (100 mW/cm^2 from a UV-Vis spot curing system). This finding was unexpected since coumarin molecules are much closer to each other in P-II for favorable dimerization. Stereo hindrance in P-II may slow down the molecular rotation to adopt the proper conformations for dimerization. The flexible linkage in P-IV prior to the coumarin sites allows the rapid adoption of favorable positions for dimerization. In addition, the elongated micelle structure in P-IV indicates the possible closer approximation of coumarin moieties via pi-pi stacking, which is favorable for coumarin dimerization. In contrast, the possible random orientation of molecules might occur within the spherical micelles formed by P-II telodendrimer before drug loading.

The crosslinking of micelle could increase the mechanical stability against the challenging environments, e.g. sodium dodecyl sulfate (SDS) incubation and physiological environments.[40] The non-crosslinked (NC) and crosslinked (C) micelles formed by P-II and P-IV were incubated with SDS and the particle sizes were analyzed via DLS. The non-crosslinked micelles were dissociated upon SDS incubation with the significantly reduced particle sizes (Figure 5D & 5H). As expected, P-IV-C could maintain the particle sizes after SDS incubation whereas the crosslinked P-II-C micelles were dissociated completely by SDS. This indicated that the coumarin dimerization in P-II-C occurred mainly between the neighboring coumarins intramolecularly due to the close proximity, which have no contribution to the micelle stability. The flexible spacers within P-IV increase the chance for

the pi-pi stacking between the intermolecular coumarins within the rod shape micelles, therefore allowing for the intermolecular coumarin dimerization to stabilize the nano-assembly. It correlates well with the observations in molecular dynamic simulations: closely stacked Co was observed in PII telodendrimer followed by pi-pi stacking with SN38; whereas, alternating Co-SN38 stacking was observed in P-IV drug loading (Figure 4).

3.4 SN-38 loading

The SN-38 loading efficiency in the telodendrimer micelles were analyzed via fluorescence quantification after removal of any drug precipitation via centrifuge and filtration through a 0.22 μm filter (Table 2). The drug loading efficiency in P-II and P-IV micelles were measured to be over 92% without any visible precipitation or big aggregates in DLS analysis. P-I and P-III micelles exhibited poor loading efficiency of 47% and 72%, respectively, with visible drug precipitations after centrifugation. This is due to the unbalanced hydrophilicity and hydrophobicity of these telodendrimers. The relatively compact oligo-Co structure in P-I decreases the efficiency of pi-pi stacking between SN-38 with Co in telodendrimer P-I. In addition, the lack of amphiphilic CA layer reduces the capability of nanocarrier to encapsulate drug. In contrast, the hydrophilic ethylene glycol linkers inserted in P-III significantly decrease the hydrophobicity of the core and lead to the loose micelle structure, which may cause drug leakage and low drug loading efficiency. As the telodendrimers P-II and P-IV showed better efficacy, they were further evaluated.

In vitro release profile of SN-38 from telodendrimer micelles were evaluated via a dialysis method against PBS and detected via fluorescence analysis. Due to the extreme poor solubility of SN-38, no free drug control could be used in the dialysis study. It was observed in Figure 6A that both P-II and P-IV micellar nanocarriers could sustain the drug familiarly with about 50% drug released on day 5 and about 85% drug released on day 20, showing a very stable drug encapsulation. The above slow SN38 release profiles via dialysis is much slower compared with paclitaxel from similar telodendrimer micelles (50% drug release at 24 h), [29] which is mainly due to the strong SN38-polymer interactions via *pi-pi* stacking, as well as the ultra low SN 38 solubility in water (0.08 μg/mL)[43]. The long-term stability of these micelle formulations at 4 °C in PBS were monitored via DLS particle sizer. SN38 loaded P-II and P-IV micelles with a drug loading of D/P=1:10 ratio were found to be stable in size around 35 to 40 nm for over one month storage (Figure 6B). The slow SN-38 drug release and the excellent stability for shelf storage do not necessarily indicate the decreased bioactivity by the reduced drug availability. Instead, the following cell culture assays revealed the completely maintained cytotoxicity in killing cancer cells. The interactions of micelles with biocomponents *in vitro* and *in vivo* will alter the drug release profile compared to the drug release by static dialysis or shelf-storage. The photo-crosslinking of P-IV micelles could increase the mechanical stability and may sustain drug release. Unfortunately, SN38 is not stable under UV treatment: color changes and partially lost of anticancer activity were observed after UV crosslinking. For this reason, no UV irradiation was applied to crosslink drug-loaded micelles in the following SN38 delivery studies. Clean reversible crosslinkable micelles may be applicable for the delivery of some other non-photosensitive drugs, such as paclitaxel, in future studies. [40]

3.5 In vitro cellular studies

In order to visualize the intracellular trafficking of micellar nanocarriers, a fluorescent dye (DiI)[44] was loaded into micelles loaded with SN38 as a surrogate for the hydrophobic payload drugs. As shown in Figure 7, free DiI quickly diffused into the mammalian cells, which was strongly hindered when the dye was embedded into the nanoparticles. The slow cell uptake of nanoformulations may be related with the slow drug release profiles, since the stealth PEG outer layer of nanoparticle slow down the cell uptake of drug-loaded nanoparticles. It potentially reduces the nonspecific cytotoxicity of the payload drug in the blood circulation. On the other hand, the cell uptake profiles of the fluorescent labeled nanoparticles P-II and P-IV both were observed to be time and concentration dependent (Figure S7), which allows for the passive EPR tumor targeting and efficient cancer treatment of nanotherapeutics.

The hemolytic properties of telodendrimers P-II and P-IV were evaluated via in vitro red blood cell incubation. Non-hemolytic properties were observed for both telodendrimers up to 1 mg/mL level after incubation at 37 °C overnight (Figure 8A). The cytotoxicity of blank P-II, P-IV micelles and SN38-loaded nanoparticles against colon cancer cells (HT-29 and HCT116) and lung cancer cells (A549) were evaluated by MTS assay after 72 h continuous incubation. As shown in Figure 8B-D, similar dose-responsive curves were observed for both SN-38 micellar formulations in all three cancer cells. The IC50 values of SN-38 loaded NPs were comparable to those of free SN-38 (in DMSO) with the ranging from 15 to 90 ng/mL, indicating SN-38 loaded NPs exhibited equivalent cytotoxic activity in vitro. Furthermore, free SN38 and SN38 loaded in NPs showed two to three orders of magnitude more toxic than the clinical pro-drug formulation of SN-38, i.e. irinotecan (Camptosar®). Additionally, there was no obvious cellular toxicity caused by the blank P-II, P-IV micelles (without SN-38) at all the tested concentrations range up to 1 mg/mL.

3.6 Fluorescence animal imaging

NIR fluorescent imaging was applied to track tumor targeting property of the nanoparticle and evaluate the *in vivo* biodistribution in nude mice bearing subcutaneous HT-29 colon cancer xenografts. A hydrophobic near-infrared (NIR) cyanine dye, DiD, was co-loaded with SN-38 into P-II and P-IV micelles at a mass ratio of 0.25/0.75/10. The fluorescence-labeled micelle preparations of P-II and P-IV had similar particle sizes of 54 and 58 nm, respectively. The mice were injected via the tail vein with the equivalent amount of free DiD dye and the DiD-SN38-loaded micelles in PBS. As shown in Figure 9A & 9B, the tumor accumulation of the DiD in the animals treated with the fluorescent P-II and P-IV nanoparticles were observed after 4 h post-injection and peaked at 24 to 48 h and maintained over the next 72 h period. In contrast, tumor targeting was not found in the tumor-bearing mice treated with the free DiD dye. The ex vivo imaging (Figure 9C & 9D) revealed that two nanoparticles clearly exhibited the highest fluorescence intensity in the tumor. Moreover, the fluorescent uptake by the liver, lung and other normal organs were very low for nanoformulation. Whereas in the mice treated with the free dye, DiD was mainly taken up by spleen, liver and lung, instead of the tumor. The duplicated small animal imaging showed the preferential tumor uptake of P-II and P-IV formulations (Figure S8).

3.7 Pharmacokinetics study

Due to the extreme low solubility of SN-38 in water, pure SN-38 was not suitable for intravenous administration, so a prodrug irinotecan was used in the PK studies, in comparison with SN-38 formulation. As shown in the in vivo imaging studies, P-IV micelles show slightly better tumor targeting than P-II formulation. Therefore, P-IV was used for the PK study. 30 mg/kg of irinotecan and the equivalent of 20 mg/kg SN38-P-IV were injected into healthy BALB/c mice through tail-vein injection and the plasma concentration of SN-38 were detected via fluorescent spectrometry. As shown in Figure 10, micelle formulation significantly delayed the blood clearance of SN-38 with the maximum detected drug concentration of 1140 μg/mL (28% of injected dose), however, only 90 μg/mL of plasma concentration (2% of injected dose) could be detected for the irinotecan at 5 min after injection. The pharmacokinetic parameters were calculated using a two compartment model with PKsolver and shown in Figure 10B. The area under the curve (AUC) for the mice treated with Irinotecan and SN38-P-IV were 465 and 166 μg.h/mL, respectively. The steady-state volume of distribution (V_{ss}) decreased in the nanoformulation by about 5 fold compared to the free drug administration, indicating the limited systemic extravasation from size effects. Compared with irinotecan, the prolonged retention and larger AUC of SN38 micellar may contribute to the better tumor targeting via EPR effect, as shown in the in vivo fluorescent imaging studies (Figure 9).

3.8 In-vivo antitumor efficacy

The anti-tumor activities of SN38 micellar formulations were evaluated in nude mice bearing subcutaneous HT-29 colon cancer xenografts in comparison with the clinical formulation of Irinotecan. According to the literature report, the dose level of 60 mg/kg was used for irinotecan in cancer treatment studies.[28] And the equivalent SN38 dose level of SN38-P-II, SN38-P-IV micelles (40 mg/kg) were administrital via tail vein injection in parallel using PBS as control (n = 5-6). Total three dosages were given every four days on days 0, 4, and 8, respectively. Animal body weight and tumor size were monitored every other day (Figure 11). Compared with the control group, prodrug irinotecan could inhibit tumor growth. SN38-P-II and SN38-P-IV showed significant better tumor inhibition throughout the treatment duration compared with both control group (P < 0.001) and irinotecan group (P < 0.005) on day 23 and 28, when tumors reached to the limit size in these groups. For example, by day 28, the median RTV was 6.4 for mice treated with Irinotecan, while the RTVs for mice treated with SN38-P-II, SN38-P-IV micelles were 3.5 and 3.0, respectively. SN38-P-IV micelles showed slightly better tumor inhibition than SN38-P-II formulation after day 24. SN38-P-II, SN38-P-IV micelles have relatively longer retention time and slow drug release profile as demonstrated earlier, which may facilitate the delivery of more SN-38 drugs to the tumor site, resulting in the improved anti-tumor efficacy. For humane reasons, animals were euthanized when the implanted tumor volume reached 1500 mm^3, which was considered as the end point of survival data. The mice survival rates were presented by the Kaplan-Meier survival curve, respectively (Figure 11B). In general, compared to PBS control, all the SN38 formulations significantly prolonged the survival rates of tumor bearing mice. The median survival time of mice in the group of PBS

control, Irinotecan, SN38-P-II and SN38-P-IV micelles were 24, 35 and 44 days, respectively.

The potential toxicities of mice after different SN38 formulations treatment were monitored by body weight change (Figure 11C) and blood cell counts (Figure 11D). Compared to PBS control group, all the animals in the treatment groups exhibited some mild body weight lost (<10%) during the injections, which was recovered a week after injections. The mice treated with SN38 nanoformulations exhibited slightly more body weight lost (10% vs 4% on day 9). On day 7 after the last injection, blood samples were collected for blood cell counts. No significant difference was observed for the RBC and WBC and hemoglobin counts between all the treatment groups and control group, which indicates no myelosuppression caused by the treatments. (Figure 11D) Platelets in the groups treated with nanoformulations were observed to increase about 70%, despite this increase platelets remained within the normal range of 592-2972 k/μL. It should be further tested in the future study whether this mild platelet increase is the sign of toxicity of the treatment.

4. Conclusions

In conclusion, several novel telodendrimers have been prepared to deliver SN38. The chemical structures, physical loading properties and the drug loading properties of these self-assembled micelles were characterized. The three-layered telodendrimers P-II and P-IV showed superior SN38 loading efficiency, capacity and stability within the self-assembled rod shape micelles and retained small particle sizes. These two telodendrimer nanocarriers were demonstrated to be non-cytotoxic and non-hemolytic up to 1 mg/mL and could release drug gradually over several days in vitro. P-II/SN38 and P-IV/SN38 increased the solubility and availability in cancer cells in vitro and showed a lower IC50 compared to free drug and about two to three magnitude lower IC50 than irinotecan. PK study and NIR fluorescence optical imaging revealed the preferred and prolonged blood circulation and specific tumor targeting properties of the SN38 nanoformulations. These two nanoformulations exhibited similar antitumor effects in HT-29 colorectal cancer xenograft models, which were significantly better than irinotecan treatment. In summary, P-II/SN38 and P-IV/38 are promising new therapeutic agents for colorectal cancer treatment. In addition, P-IV is attractive for further development because of the interesting photo-redox dual sensitivity to reversibly crosslink nanocarrier for the on-demand anticancer drug delivery.

Supplementary Material

Refer to Web version on PubMed Central for supplementary material.

Acknowledgments

References

1. Ferlay J, Shin HR, Bray F, Forman D, Mathers C, Parkin DM. Estimates of worldwide burden of cancer in 2008: GLOBOCAN 2008. Int J Cancer. 2010; 127:2893–917. [PubMed: 21351269]

2. Siegel R, Naishadham D, Jemal A. Cancer statistics, 2013. CA Cancer J Clin. 2013; 63:11–30. [PubMed: 23335087]

3. Pizzolato JF, Saltz LB. The camptothecins. Lancet. 2003; 361:2235–42. [PubMed: 12842380]

4. Cunningham D, Pyrhonen S, James RD, Punt CJ, Hickish TF, Heikkila R, et al. Randomised trial of irinotecan plus supportive care versus supportive care alone after fluorouracil failure for patients with metastatic colorectal cancer. Lancet. 1998; 352:1413–8. [PubMed: 9807987]

5. Saltz LB, Cox JV, Blanke C, Rosen LS, Fehrenbacher L, Moore MJ, et al. Irinotecan plus fluorouracil and leucovorin for metastatic colorectal cancer. Irinotecan Study Group. N Engl J Med. 2000; 343:905–14. [PubMed: 11006366]

6. Noda K, Nishiwaki Y, Kawahara M, Negoro S, Sugiura T, Yokoyama A, et al. Irinotecan plus cisplatin compared with etoposide plus cisplatin for extensive small-cell lung cancer. N Engl J Med. 2002; 346:85–91. [PubMed: 11784874]

7. Negoro S, Masuda N, Takada Y, Sugiura T, Kudoh S, Katakami N, et al. Randomised phase III trial of irinotecan combined with cisplatin for advanced non-small-cell lung cancer. Br J Cancer. 2003; 88:335–41. [PubMed: 12569373]

8. Bodurka DC, Levenback C, Wolf JK, Gano J, Wharton JT, Kavanagh JJ, et al. Phase II trial of irinotecan in patients with metastatic epithelial ovarian cancer or peritoneal cancer. J Clin Oncol. 2003; 21:291–7. [PubMed: 12525521]

9. Senter PD, Beam KS, Mixan B, Wahl AF. Identification and activities of human carboxylesterases for the activation of CPT-11, a clinically approved anticancer drug. Bioconjug Chem. 2001; 12:1074–80. [PubMed: 11716702]

10. Combes O, Barre J, Duche JC, Vernillet L, Archimbaud Y, Marietta MP, et al. In vitro binding and partitioning of irinotecan (CPT-11) and its metabolite, SN-38, in human blood. Invest New Drugs. 2000; 18:1–5. [PubMed: 10830136]

11. Bleiberg H. CPT-11 in gastrointestinal cancer. Eur J Cancer. 1999; 35:371–9. [PubMed: 10448285]

12. Bala V, Rao S, Boyd BJ, Prestidge CA. Prodrug and nanomedicine approaches for the delivery of the camptothecin analogue SN38. J Control Release. 2013; 172:48–61. [PubMed: 23928356]

13. Duncan R. Polymer therapeutics as nanomedicines: new perspectives. Curr Opin Biotechnol. 2011; 22:492–501. [PubMed: 21676609]

14. Zhang H, Wang J, Mao W, Huang J, Wu X, Shen Y, et al. Novel SN38 conjugate-forming nanoparticles as anticancer prodrug: in vitro and in vivo studies. J Control Release. 2013; 166:147–58. [PubMed: 23266448]

15. Sapra P, Zhao H, Mehlig M, Malaby J, Kraft P, Longley C, et al. Novel delivery of SN38 markedly inhibits tumor growth in xenografts, including a camptothecin-11-refractory model. Clin Cancer Res. 2008; 14:1888–96. [PubMed: 18347192]

16. Pal A, Khan S, Wang YF, Kamath N, Sarkar AK, Ahmad A, et al. Preclinical safety, pharmacokinetics and antitumor efficacy profile of liposome-entrapped SN-38 formulation. Anticancer Res. 2005; 25:331–41. [PubMed: 15816556]

17. Vijayalakshmi N, Ray A, Malugin A, Ghandehari H. Carboxyl-terminated PAMAM-SN38 conjugates: synthesis, characterization, and in vitro evaluation. Bioconjug Chem. 2010; 21:1804–10. [PubMed: 20836544]

18. Matsumura Y. Preclinical and clinical studies of NK012, an SN-38-incorporating polymeric micelles, which is designed based on EPR effect. Adv Drug Deliv Rev. 2011; 63:184–92. [PubMed: 20561951]

19. Vangara KK, Liu JL, Palakurthi S. Hyaluronic acid-decorated PLGA-PEG nanoparticles for targeted delivery of SN-38 to ovarian cancer. Anticancer Res. 2013; 33:2425–34. [PubMed: 23749891]

20. Koizumi F, Kitagawa M, Negishi T, Onda T, Matsumoto S, Hamaguchi T, et al. Novel SN-38-incorporating polymeric micelles, NK012, eradicate vascular endothelial growth factor-secreting bulky tumors. Cancer Res. 2006; 66:10048–56. [PubMed: 17047068]

21. Hamaguchi T, Doi T, Eguchi-Nakajima T, Kato K, Yamada Y, Shimada Y, et al. Phase I study of NK012, a novel SN-38-incorporating micellar nanoparticle, in adult patients with solid tumors. Clin Cancer Res. 2010; 16:5058–66. [PubMed: 20943763]

22. Kedar U, Phutane P, Shidhaye S, Kadam V. Advances in polymeric micelles for drug delivery and tumor targeting. Nanomedicine. 2010; 6:714–29. [PubMed: 20542144]

23. Oerlemans C, Bult W, Bos M, Storm G, Nijsen JF, Hennink WE. Polymeric micelles in anticancer therapy: targeting, imaging and triggered release. Pharm Res. 2010; 27:2569–89. [PubMed: 20725771]

24. Soppimath KS, Aminabhavi TM, Kulkarni AR, Rudzinski WE. Biodegradable polymeric nanoparticles as drug delivery devices. J Control Release. 2001; 70:1–20. [PubMed: 11166403]

25. Yokoyama M. Polymeric micelles as a new drug carrier system and their required considerations for clinical trials. Expert Opin Drug Deliv. 2010; 7:145–58. [PubMed: 20095939]

26. Iyer AK, Greish K, Seki T, Okazaki S, Fang J, Takeshita K, et al. Polymeric micelles of zinc protoporphyrin for tumor targeted delivery based on EPR effect and singlet oxygen generation. J Drug Target. 2007; 15:496–506. [PubMed: 17671896]

27. Caron WP, Song G, Kumar P, Rawal S, Zamboni WC. Interpatient pharmacokinetic and pharmacodynamic variability of carrier-mediated anticancer agents. Clin Pharmacol Ther. 2012; 91:802–12. [PubMed: 22472987]

28. Carie A, Rios-Doria J, Costich T, Burke B, Slama R, Skaff H, et al. IT-141, a Polymer Micelle Encapsulating SN-38, Induces Tumor Regression in Multiple Colorectal Cancer Models. J Drug Deliv. 2011; 2011:869027. [PubMed: 22187652]

29. Luo J, Xiao K, Li Y, Lee JS, Shi L, Tan YH, et al. Well-defined, size-tunable, multifunctional micelles for efficient paclitaxel delivery for cancer treatment. Bioconjug Chem. 2010; 21:1216–24. [PubMed: 20536174]

30. Huang W, Shi C, Shao Y, Lam KS, Luo J. The core-inversible micelles for hydrophilic drug delivery. Chem Commun. 2013; 49:6674–6.

31. Xiao K, Luo J, Fowler WL, Li Y, Lee JS, Xing L, et al. A self-assembling nanoparticle for paclitaxel delivery in ovarian cancer. Biomaterials. 2009; 30:6006–16. [PubMed: 19660809]

32. Li Y, Xiao W, Xiao K, Berti L, Luo J, Tseng HP, et al. Well-defined, reversible boronate crosslinked nanocarriers for targeted drug delivery in response to acidic pH values and cis-diols. Angew Chem Int Ed Engl. 2012; 51:2864–9. [PubMed: 22253091]

33. Baek HG, Liu R, Lam KS. Development of hydrogel TentaGel shell-core beads for ultrahigh throughput solution-phase screening of encoded OBOC combinatorial small molecule libraries. J Comb Chem. 2009; 11:91–102. [PubMed: 19061339]

34. He J, Zhao Y, Zhao Y. Photoinduced bending of a coumarin-containing supramolecular polymer. Soft Matter. 2009; 5:308–10.

35. Bowers, KJ.; Chow, E.; Huageng, X.; Dror, RO.; Eastwood, MP.; Gregersen, BA., et al. Scalable Algorithms for Molecular Dynamics Simulations on Commodity Clusters; SC 2006 Conference, Proceedings of the ACM/IEEE; 2006. p. 43

36. Shan Y, Kim ET, Eastwood MP, Dror RO, Seeliger MA, Shaw DE. How Does a Drug Molecule Find Its Target Binding Site? J Am Chem Soc. 2011; 133:9181–3. [PubMed: 21545110]

37. Berendsen, HJC.; Postma, JPM.; van Gunsteren, WF.; Hermans, J. Interaction Models for Water in Relation to Protein Hydration. In: Pullman, B., editor. Intermolecular Forces. Springer; Netherlands: 1981. p. 331-42.

38. Essmann U, Perera L, Berkowitz ML, Darden T, Lee H, Pedersen LG. A smooth particle mesh Ewald method. J Chem Phys. 1995; 103:8577–93.

39. Jiang J, Qi B, Lepage M, Zhao Y. Polymer Micelles Stabilization on Demand through Reversible Photo-Cross-Linking. Macromolecules. 2007; 40:790–2.

40. Shao Y, Shi C, Xu G, Guo D, Luo J. Photo and redox dual responsive reversibly cross-linked nanocarrier for efficient tumor-targeted drug delivery. ACS Appl Mater Interfaces. 2014; 6:10381–92. [PubMed: 24921150]

41. Israelachvili, JN. Intermolecular and Surfaces Forces. 2nd. London: Academic Press; 1992.

42. Gohy JF, Zhao Y. Photo-responsive block copolymer micelles: design and behavior. Chem Soc Rev. 2013; 42:7117–29. [PubMed: 23364156]

43. Vangara KK, Ali HI, Lu D, Liu JL, Kolluru S, Palakurthi S. SN-38-cyclodextrin complexation and its influence on the solubility, stability, and in vitro anticancer activity against ovarian cancer. AAPS PharmSciTech. 2014; 15:472–82. [PubMed: 24477982]

44. Bastiat G, Pritz CO, Roider C, Fouchet F, Lignieres E, Jesacher A, et al. A new tool to ensure the fluorescent dye labeling stability of nanocarriers: a real challenge for fluorescence imaging. J Control Release. 2013; 170:334–42. [PubMed: 23792117]

45. Zhang Y, Huo M, Zhou J, Xie S. PKSolver: An add-in program for pharmacokinetic and pharmacodynamic data analysis in Microsoft Excel. Comput Meth and Prog in Biomed. 2010; 99:306–14.
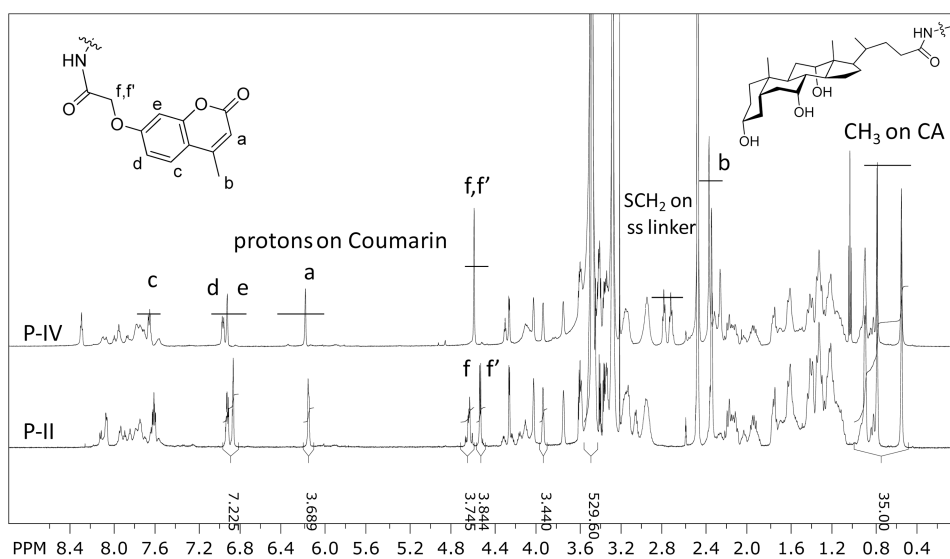
Figure 1.
^{1}H NMR spectra of P-II and P-IV recorded in DMSO-d_6. The chemical compositions of telodendrimers were calculated based on the peak integrations of signature signals of Co and CA relative to the signals of MeOPEG.
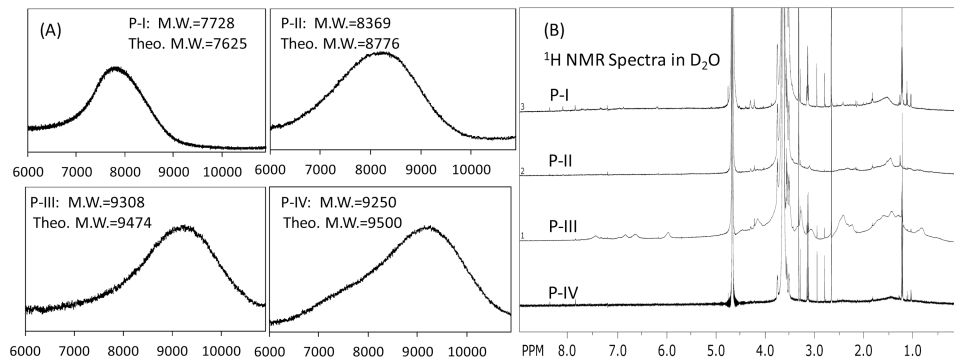
Figure 2.
(A) MALDI-TOF MS spectra of telodendrimers P-I, P-II, P-III and P-IV; (B) ^{1}H NMR spectra of telodendrimers P-I, P-II, P-III and P-IV in D$_2$O, the significant suppression of the hydrophobic building blocks and the good detection of hydrophilic PEG indicated the formation of core-shell structure of micelles.
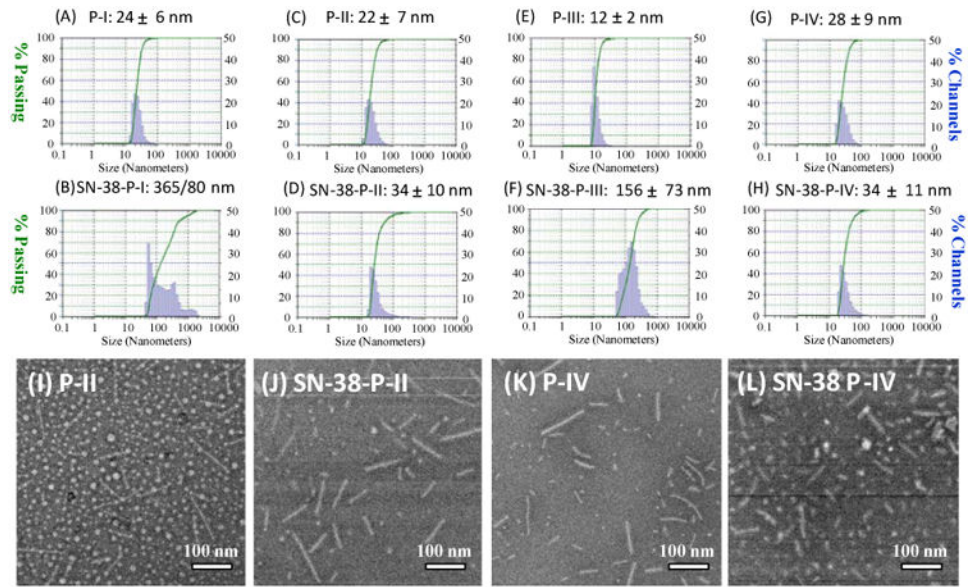
Figure 3.
(A-H) Particle sizes of P-I, P-II, P-III and P-IV by DLS, before and after SN-38 loading at a 1:10 drug/polymer ratio. (I-L) The TEM images of the empty and SN-38 loaded P-II and P-IV micelles.
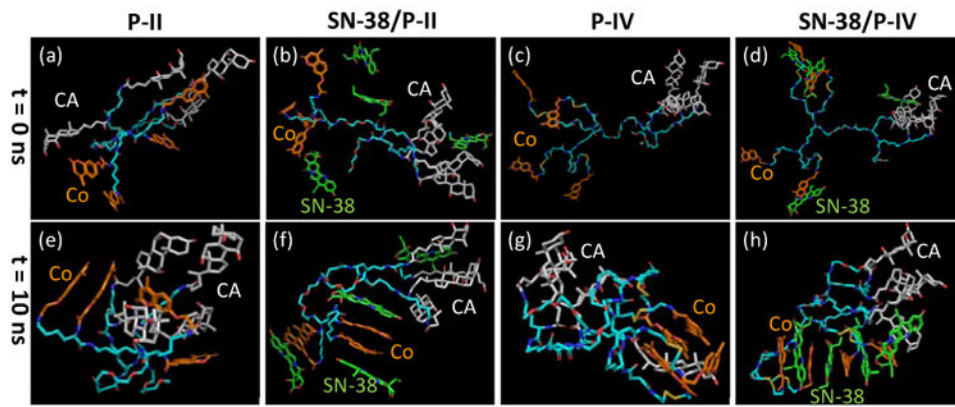
Figure 4.
The conformations of the telodendrimer P-II and P-IV and the complex with four SN38 molecules obtained before and after molecular dynamic simulation (t = 10 ns). PEG chain was not included in the MD simulation.
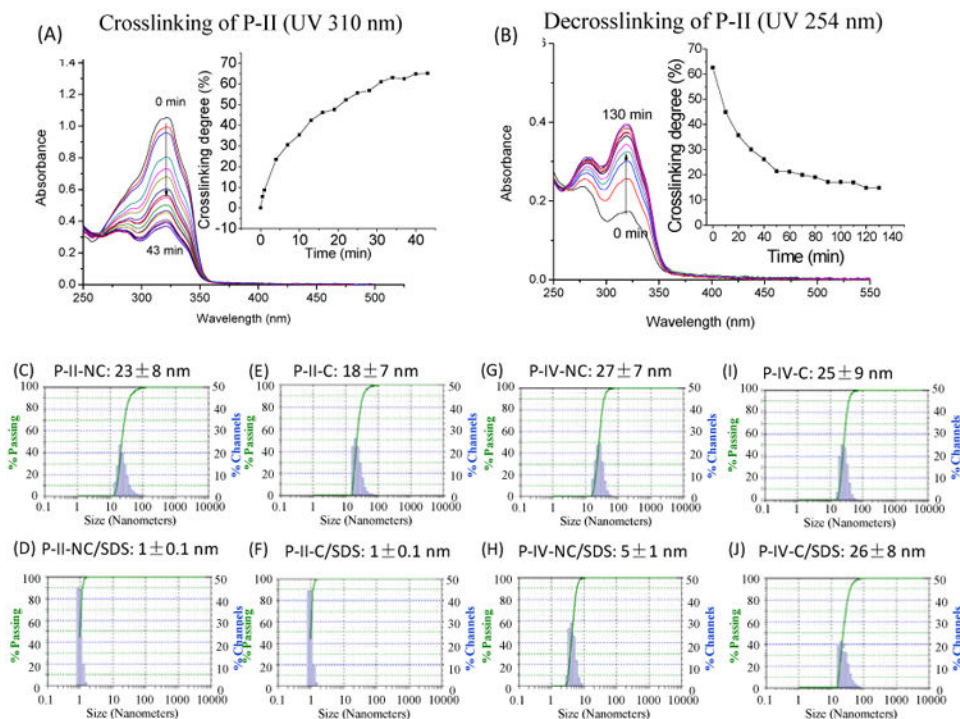
Figure 5.
(A) Photo-crosslinking and (B) photo-de-crosslinking of telodendrimer micelles P-II via UV irradiation at 310 and 254 nm, respectively. The crosslinking degree was monitored the absorbance changes at 320 nm, which is the signature absorbance of the coumarin monomer. (C-J) the particles sizes of the crosslinked and non-crosslinked P-II and P-IV micelles in PBS or incubated with SDS. The final concentrations of polymer and SDS were 1 and 2.5 mg/mL, respectively.
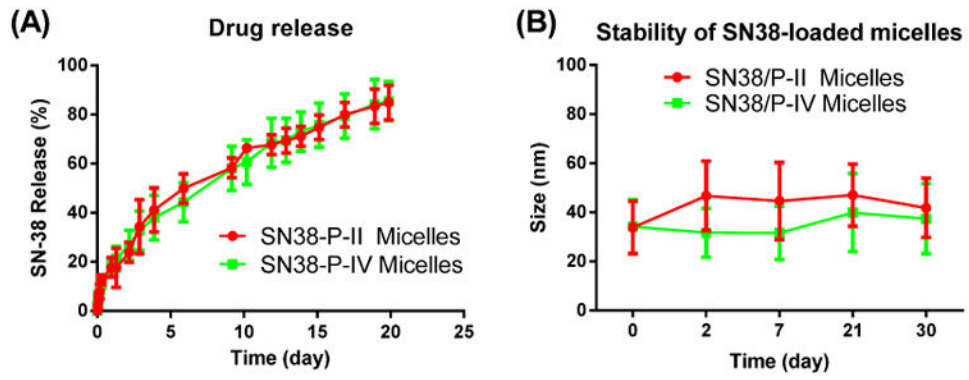
Figure 6.
(A) SN-38 release profiles from P-II and P-IV telodendrimer nanocarriers; (B) The stability of the particle sizes for SN-38 loaded P-II and P-IV micelles upon storage in PBS at 4°C.
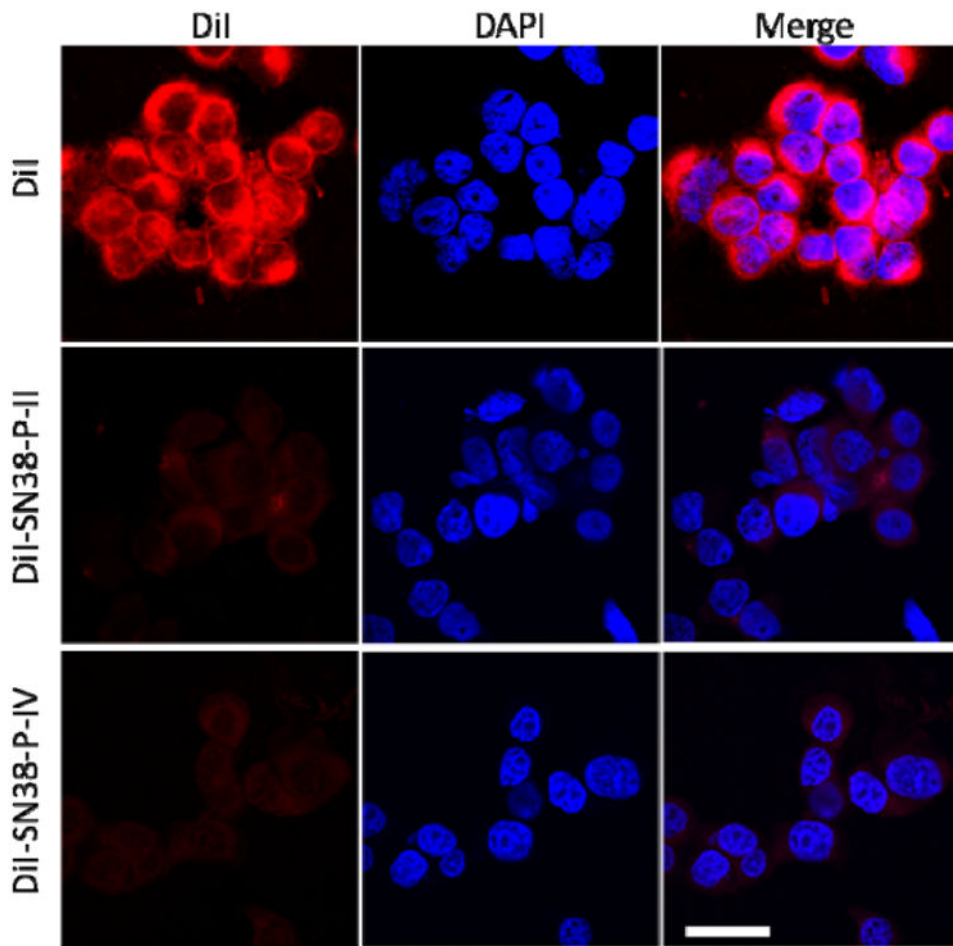
Figure 7.
Confocal fluorescence microscopy images of HT-29 cells incubated with 1 µg/mL of free DiI and DiI-SN38 co-loaded micelles at 37 °C for 2 h. Cell nuclear was stained with DAPI (Blue). Scale bar: 30 µm.
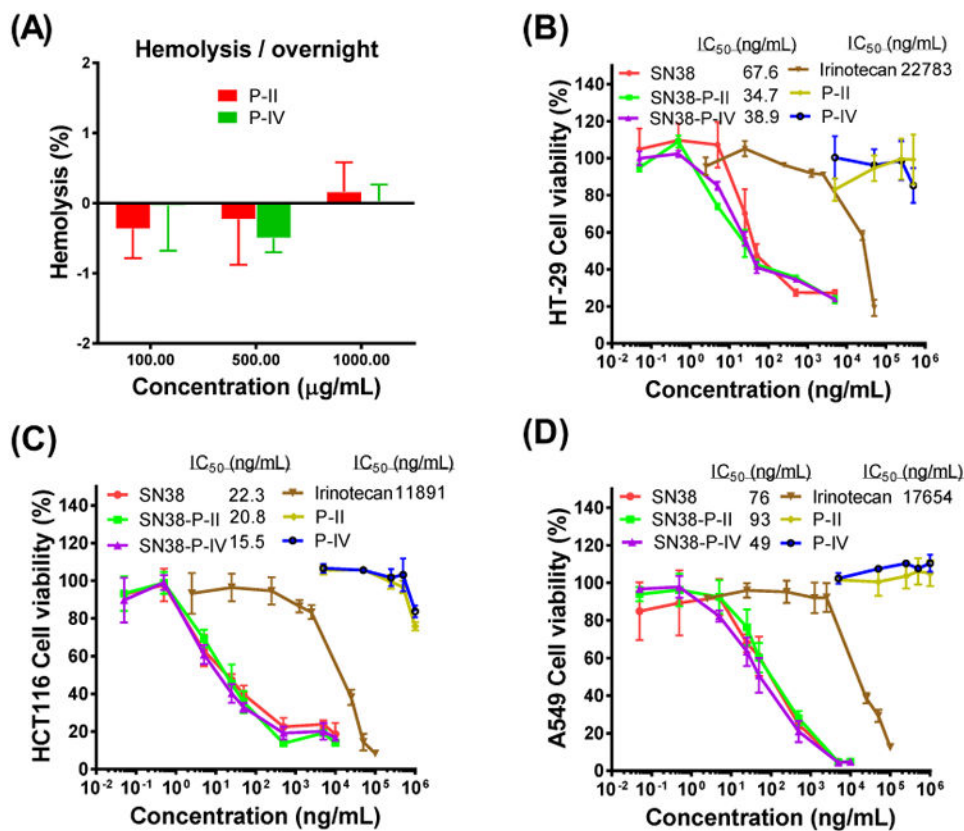
Figure 8.
(A) The hemolysis properties of telodendrimer P-II and P-IV at different concentrations after incubation with red blood cells at 37 °C overnight. The cell viability of HT-29 (B), HCT116 (C) colon cancer cells and A549 (D) lung cancer cells after incubation for 72 h with blank and SN-38-loaded P-II and P-IV micelles, compared with free SN-38 and irinotecan.
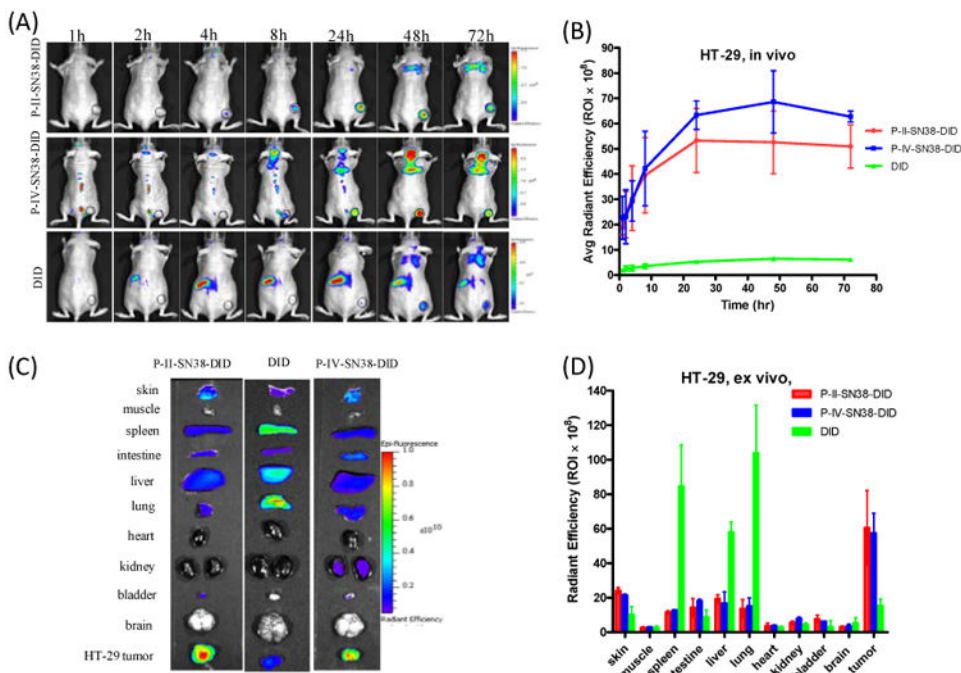
Figure 9.
In vivo and ex vivo NIRF imaging of P-II, P-IV nanoparticles biodistribution after i.v. injection in subcutaneous HT-29 colon tumor bearing mice. (A) In vivo optical images of real-time tumor targeting characteristics of DiD-SN38-loaded P-II, P-IV micelles. Tumor bearing mice were injected i.v. with the equivalent amount of free DiD dye or DiD-SN38 nanoparticles; (B) Time-dependent tumor accumulation profile of DiD-SN38-NPs (n = 2). (C) Representative ex vivo optical images of tumors and organs of HT-29 colon cancer bearing mice sacrificed at 72 h. (D) quantitative fluorescence intensities of tumors and organs from ex vivo images (n = 2).

(A)

(B)

Parameters	SN38-P-IV	Irinotecan
C_{max}^{a} (µg/mL)	1140	90
CL (mL/kg/h)	85.97	336.1
CL2 (mL/kg/h)	1187.64	210.39
AUC (µg/mL*h)	465.28	166.11
Vss (mL/kg)	25.20	124.19
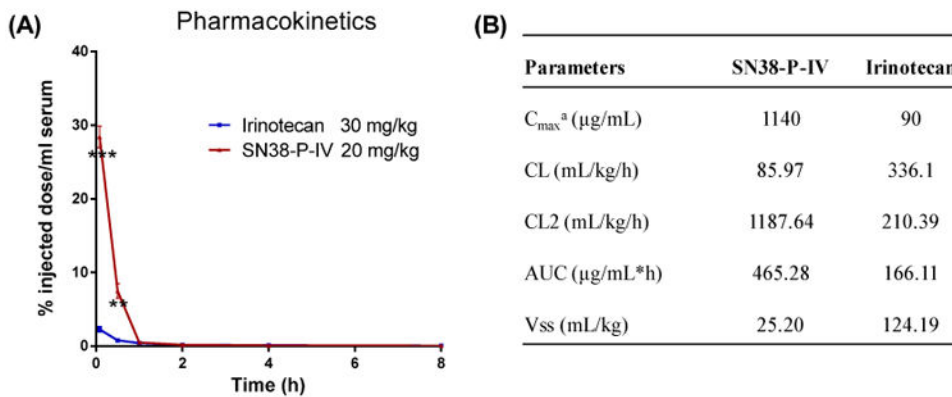
Figure 10.
Pharmacokinetics of SN38-P-IV and ironitecan injected i.v. at a dose of 20 mg/kg SN-38 equivalent, respectively; (B) Pharmacokinetic parameter estimations of SN38 concentration health BALB/c mice. Note: The pharmacokinetic parameters were calculated using a two compartment model with PKsolver, an add-in program in Microsoft Excel.[45] ^{a} C_{max} represents the maximum observed concentration at the earliest evaluated time point of 5 min post *iv* injection; Plasma concentration at 0 h time point were calculated based on the dose levels. **Abbreviations:** $t_{1/2}$, half life time; C_{max}, maximum platinum concentration; AUC, area under the curve; Cl, clearance; V_{ss}, steady-state volume of distribution.
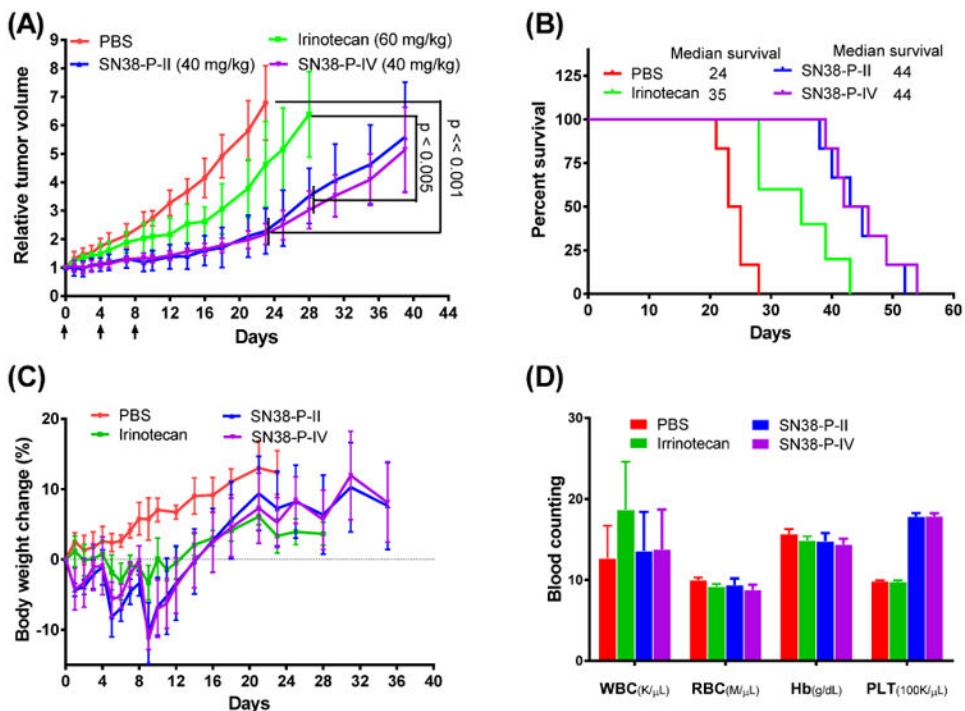
Figure 11.
(A) *In vivo* anti-tumor efficacy, (B) survival data and (C) body weight changes after intravenous treatment via different SN38 formulations in the nude mice bearing subcutaneous HT-29 colon cancer tumor xenografts (n = 5-6). (D) The blood counting analysis of the animals on day 7 after the last injection.
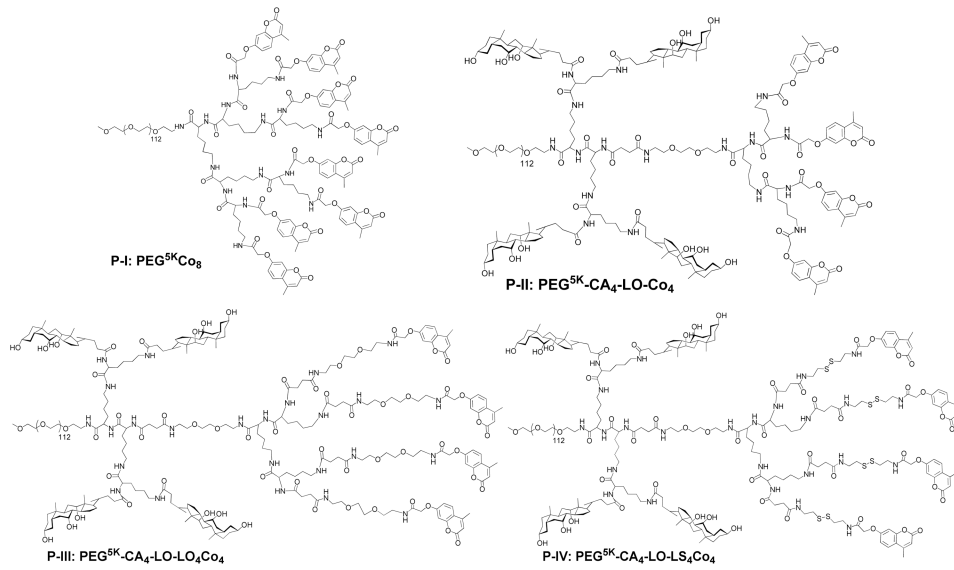
Scheme 1.
Chemical structures of telodendrimers P-I, P-II, P-III and P-IV with different architectures and linker molecules.

Table 1

Characteristics of Telodendrimers P-I, P-II, P-III, P-IV

Polymer	Formula (Theo.)	Formula (NMR)	Mw (Da)		CMC (μM)	Size (nm)
			Theo.	MS		
P-I	$PEG^{5K}Co_8$	$PEG^{5K}Co_8$	7625	7728	3.2	24 ± 6
P-II	$PEG^{5K}-CA_4-LO-Co_4$	$PEG^{5K}CA_{3.33}-LO-Co_{3.94}$	8776	8369	1.9	22 ± 7
P-III	$PEG^{5K}-CA_4-LO-LO_4Co_4$	$PEG^{5K}-CA_{3.0}-LO-LO_4Co_{3.6}$	9474	9308	4.5	12 ± 2
P-IV	$PEG^{5K}-CA_4-LO-LS_4Co_4$	$PEG^{5K}-CA_{3.96}-LO-LS_4Co_{3.91}$	9500	9250	1.3	28 ± 9

Table 2

Characteristics of SN-38 loaded micelles.

SN-38 loaded micelles	D/P ratio[a]	DLE (%)[b]	DLC (%)[c]	Mean size/nm[d]
SN38/P-I	1/10	47.3±1.6	4.52	51 ±19[e]
SN38/P-II	1/10	92.3±4.3	8.45	34 ±10
SN38/P-III	1/10	72.4±3.9	6.75	156 ± 73
SN38/P-IV	1/10	92.9±1.9	8.50	34 ±11

[a]D/P ratio= weight of SN-38/weight of polymer.

[b]Drug (SN-38) loading efficiency (%)= (weight of SN-38 in the micelles/weight of total SN-38 in the loading solution) ×100. Data were obtained from triplicate experiments.

[c]Drug loading content (%)= weight of SN-38/(weight of SN-38+ weight of polymer) ×100.

[d]Determined by dynamic light scattering (DLS).

[e]After remove precipitation by filtration.